Orbital Longitudinal Magnetoelectricity in Quasi-2D Parity-Violating Antiferromagnets: Interplay of Berry Phase and Stacking Order

Jin-Xin Hu^{1,2,*}

¹Division of Physics and Applied Physics, School of Physical and Mathematical Sciences, Nanyang Technological University, Singapore 637371 ²Department of Physics, Hong Kong University of Science and Technology, Clear Water Bay, Hong Kong, China

The magnetoelectric (ME) effect traditionally arises from complex spin-orbital interactions in multiferroic materials. In this work, we propose a distinct, intrinsic mechanism for the magnetoelectric effect in quasi-2D magnetic systems that lack spatial inversion symmetry. We demonstrate that in such parity-violating magnets, the stacking order, which id coupled with Berry curvature and orbital magnetic moment, generates a stacking Berry curvature dipole (SBCD) and a stacking orbital magnetic moment dipole (SOMD). The SBCD and SOMD act as fundamental ingredients of the ME response. As concrete examples, we apply our framework to antiferromagnets such as monolayer Ca(CoN)₂ and multilayer MnBi₂Te₄ with stacking magnetic orders. Our results reveal the microscopic orbital origin of the ME effect in antiferromagnetic systems with vanishing net Berry curvature and orbital magnetization, governed by the interplay between layer stacking, Berry curvature, and magnetic order. The SBCD is also identified as the origin of electric-field-induced Hall effects.

Introduction.—The magnetoelectric (ME) effect describes the generation of magnetization by an electric field and of electric polarization by a magnetic field [1– 4]. This cross-coupling offers a promising paradigm for next-generation electronic devices, as it enables efficient control of magnetic and electric orders, which is a central objective for low-energy-consumption spintronics [5– 7]. Historically, the ME effect has been extensively studied in three-dimensional (3D) single-phase multiferroics such as Cr₂O₃ [8] and BiFeO₃ [9, 10], where it typically arises from relativistic spin-orbit coupling and complex spin-lattice interactions [11, 12]. In recent years, interests have grown in the topological origin of the magnetoelectric (ME) effect, including the gyrotropic ME effect [13, 14] and topological ME responses [15, 16]. The former stems from the orbital magnetic moment on the Fermi surface, while the latter arises from the Chern-Simons term.

The recent discovery of intrinsic magnetism in van der Waals (vdW) materials, such as CrI₃ and MnBi₂Te₄, has opened a new frontier in exploring low-dimensional magnetism [17–28]. A key feature of these quasi-2D systems is their unique layer stacking order, which typically breaks spatial inversion symmetry (\mathcal{P}) . When combined with magnetic order that breaks time-reversal symmetry (T), this stacking establishes the fundamental prerequisite for a linear magnetoelectric effect [29, 30]. The modern theory of the ME effect focuses on axion coupling in three-dimensional (3D) systems. For instance, the ME coefficient is quantized to $e^2/2h$ in axion insulators [31, 32]. In parallel, the role of Berry phase effects in electronic transport, such as the anomalous Hall effect [33, 34], its nonlinear counterpart [35] and orbital magnetization [36, 37], has been extensively studied. Upto date, the role of the Berry phase in linear magnetoelectric phenomena, particularly in quasi-2D magnetic

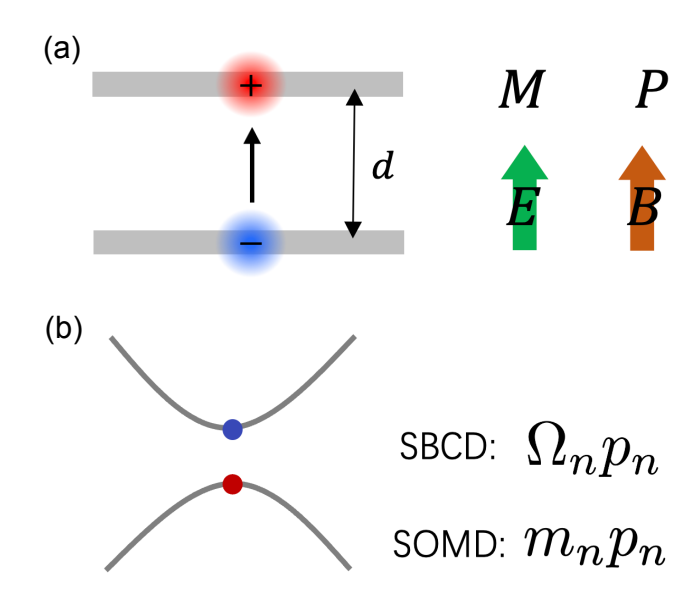


FIG. 1. (a) Schematic illustration of the longitudinal ME effect in a bilayer system. The interlayer distance is d. Under the applied magnetic (B) field and electric (E) field, the electric polarization and magnetization can be induced. (b) The stacking Berry curvature dipole (SBCD) and stacking orbital magnetic moment dipole (SOMD) are centralized near the band edge, which give rise to the orbital ME effect.

systems, remains largely unexplored.

In this work, we elucidate the orbital origin of the ME coupling in non-centrosymmetric quasi-2D antiferromagnetic materials with vanishing total Berry curvature and orbital magnetization. Focusing on systems with combined symmetries such as \mathcal{PT} symmetry, we demonstrate that the stacking Berry curvature dipole (SBCD) and the stacking orbital magnetic dipole (SOMD) are two universal quantities for intrinsic magnetoelectricity in such

systems. We posit that the layer stacking order creates a synthetic dimension in which a dipole moment of Berry curvature (orbital magnetic moment) can develop; this dipole is directly modulated by the magnetic order. This mechanism provides a purely electronic, intrinsic origin for the ME effect, distinct from other extrinsic mechanisms.

This work is structured as follows. First, we present a general microscopic theory for longitudinal ME coupling in quasi-2D systems. We emphasize that unlike multilayer graphene, the SBCD and SOMD govern the longitudinal ME coupling in antiferromagnetic systems with vanishing Berry curvature and orbital magnetization. Second, we apply our general theory to a model with symmetry $C_{4z}\mathcal{PT}$, which can describe a monolayer of Ca(CoN)₂ [39]. Furthermore, we also study a topological antiferromagnet bilayers with the prototypical material MnBi₂Te₄. Here, finite interlayer coupling causes the ME coefficient in the insulating regime to deviate from the half-quantized value. Finally, we summarize our findings and discuss the distinct origins of the ME effect in various van der Waals (vdW) magnets. This work establishes a comprehensive picture of longitudinal ME effects in vdW heterostructures, and the general formalism can be readily applied to DFT calculations.

General theory of longitudinal ME coupling—The linear magnetoelectric coupling is described microscopically by $\delta M = \chi_{\rm me} E$ and $\delta P = \chi_{\rm em} B$, where δM is the induced magnetization, δP is the induced polarization, and E and B are the applied electric and magnetic fields, respectively. In the following, we focus on the geometry where all fields, polarizations, and magnetizations are oriented out-of-plane. The linear magnetoelectric coefficients are denoted $\chi_{\rm me}$ and $\chi_{\rm em}$, and a Maxwell relation ensures $\chi_{\rm em} = \chi_{\rm me}$. For simplicity we take $\Delta = edE$ to denote the vertical electric field.

For quasi-2D layered systems, the linear ME coefficient is given by [38]

$$\chi_{\text{me}} = e \sum_{n\mathbf{k}} \left\{ -\alpha_{n\mathbf{k}} f_{n\mathbf{k}} + m_{n\mathbf{k}} p_{n\mathbf{k}} f'_{n\mathbf{k}} + \frac{e}{\hbar} \left[\delta_{\Delta} \Omega_{n\mathbf{k}} \phi(\varepsilon_{n\mathbf{k}}) / \beta - \Omega_{n\mathbf{k}} f_{n\mathbf{k}} p_{n\mathbf{k}} \right] \right\},$$
(1)

where n, \mathbf{k} are the band index and wavevector, $\phi(\varepsilon) = \ln[1 + e^{-\beta(\varepsilon-\mu)}]$ and $f_{n\mathbf{k}} = -\partial_{\epsilon}\phi(\epsilon)/\beta = \{1 + \exp[\beta(\varepsilon_{n\mathbf{k}} - \mu)]\}^{-1}$ is the Fermi-Dirac function. The first term in Eq. (1) is the orbital ME moment $\alpha_{n\mathbf{k}} \approx -\delta_{\Delta}m_{n\mathbf{k}}$ that governs ME effect in multilayer graphene [38]. The magnetic moment polarizability $\delta_{\Delta}m_{n\mathbf{k}}$ and Berry curvature polarizability $\delta_{\Delta}\Omega_{n\mathbf{k}}$ can be obtained as

$$\delta_{\Delta} m_{n\mathbf{k}} = -\sum_{m \neq n} \frac{e\hbar}{\varepsilon_{nm}^2} \operatorname{Im} \left[\varepsilon_{nm} \delta_{\Delta} \mathbf{v}_{nm} \times \mathbf{v}_{mn} + v_{nm}^x v_{mn}^y (p_m - p_n) \right], \tag{2}$$

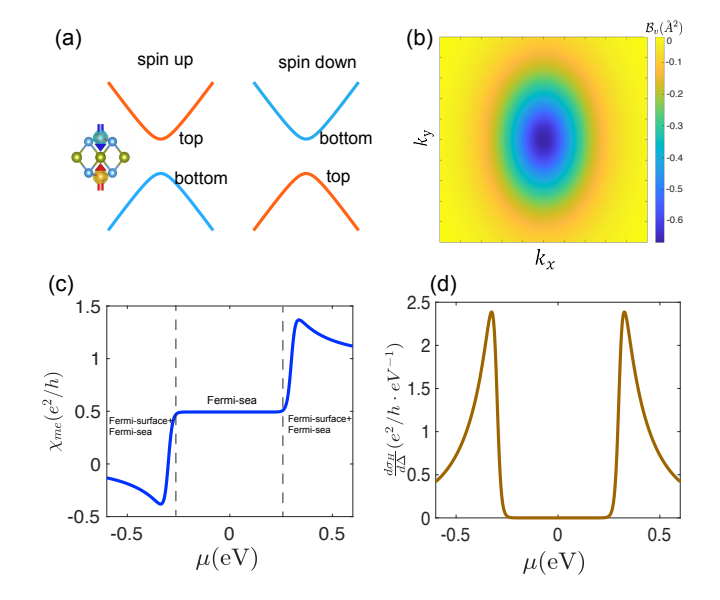


FIG. 2. (a) Schematic of the low-energy band structure with $C_{4z}\mathcal{PT}$ symmetry, illustrating the spin-layer locking. The X and Y valleys correspond to spin-up and spin-down states, respectively. The side panel shows magnetic moments localized primarily on the top and bottom Co atoms, aligned in opposite directions. (b) Momentum-space distribution of the Berry curvature component \mathcal{B}_{vk} . (c) Calculated magnetoelectric coefficient χ me as a function of Fermi energy μ . (d) Response of the electric Hall conductivity, $d\sigma_H/d\Delta$. Parameters for the model: $(v_1, v_2) = (0.6, 0.4) \mathrm{eV} \cdot \mathring{A}$ and $\Delta = 0.3 \mathrm{eV}$.

and

$$\delta_{\Delta}\Omega_{n\mathbf{k}} = -\sum_{m\neq n} \frac{2\hbar^2}{\varepsilon_{nm}^3} \operatorname{Im}\left[\varepsilon_{nm}\delta_{\Delta}\mathbf{v}_{nm} \times \mathbf{v}_{mn} + 2v_{nm}^x v_{mn}^y (p_m - p_n)\right], \tag{3}$$

where we have recalled $\Omega_{n\mathbf{k}} = i \sum_{m \neq n} \mathbf{r}_{nm} \times \mathbf{r}_{mn}$. Here $\delta_{\Delta} \mathbf{v}_{nm} = \sum_{q \neq n} p_{nq} \mathbf{v}_{qm} / \varepsilon_{nq} + \sum_{l \neq m} p_{lm} \mathbf{v}_{nl} / \varepsilon_{ml}$. The layer polarization operator \hat{p} is generally given by

$$\hat{p} = \sum_{\ell,\alpha} (\ell/d) |\phi_{\ell,\alpha}\rangle \langle \phi_{\ell,\alpha}| \tag{4}$$

where $|\phi_{\ell,\alpha}\rangle$ denotes the α orbital on the layer at height ℓ measured from the center of the stack. For example, for a bilayer system $\ell = (d/2)\{-1,1\}$ and $\hat{p} = \sigma_z/2$.

For antiferromagnetic ystems with vanishing Berry curvature and orbital moment, we have

$$\chi_{\text{me}} = e \sum_{n\mathbf{k}} \mathcal{M}_{n\mathbf{k}} f'_{n\mathbf{k}} - \frac{e}{\hbar} \mathcal{B}_{n\mathbf{k}} f_{n\mathbf{k}}, \tag{5}$$

Where we have defined the SBCD $\mathcal{B}_{nk} = \Omega_{nk} p_{nk}$ and SOMD $\mathcal{M}_{nk} = m_{nk} p_{nk}$. Eq. (5) is the main result of this work. It is clear that the first term is Fermi surface effect governed by \mathcal{M}_{nk} , while the second term is Fermi sea effect governed by \mathcal{B}_{nk} . It is important to note that both \mathcal{B}_{nk} and \mathcal{M}_{nk} survives \mathcal{PT} symmetry. The $\delta_{\Delta} m$

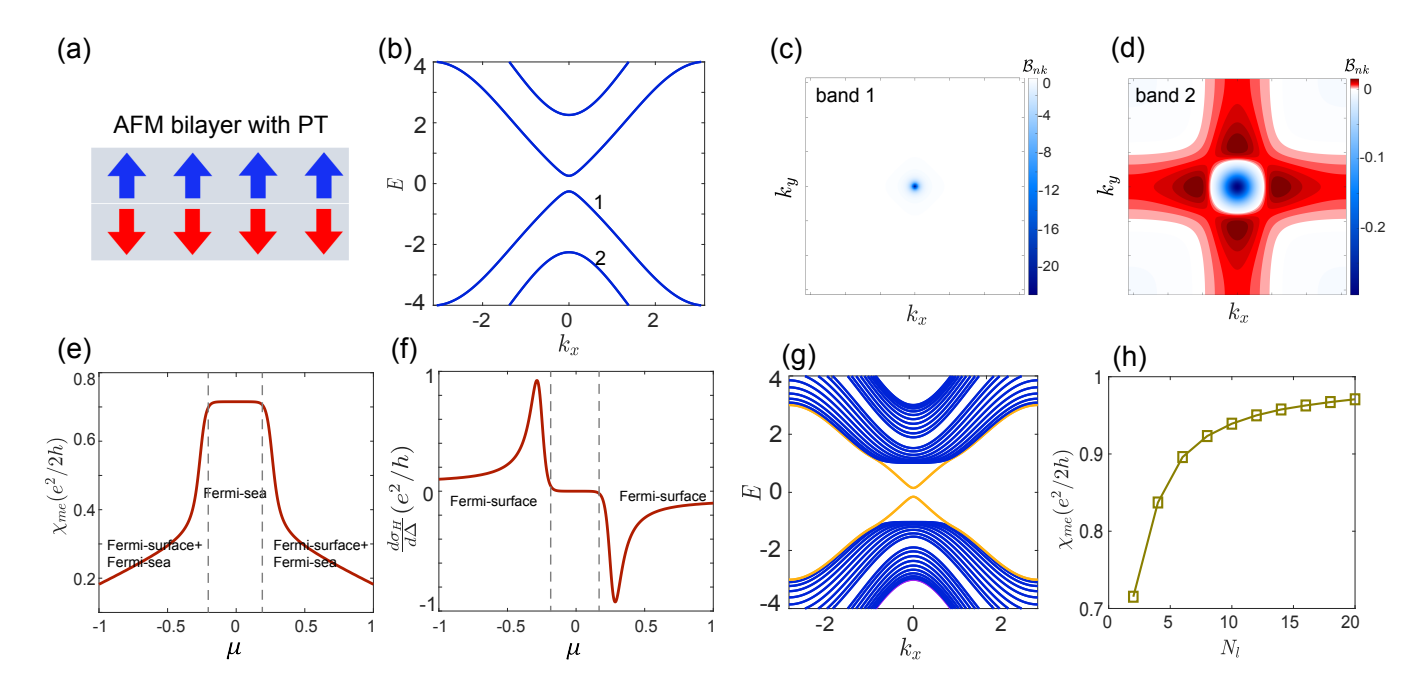


FIG. 3. (a) Schematic plot of the AFM bilayers with \mathcal{PT} symmetry and interlayer AFM order. (b) The band structure for $N_l=2$. (c) and (d) The k-space SBCD B_{nk} for the band 1 and 2 in (b). (e) The ME coefficient χ_{me} as a function if μ in the low-energy regime. Both Fermi-surface and Fermi-sea terms are shown. (f) The electric Hall effect $d\sigma_H/d\Delta$ as a function if μ . (g) The band structure of multilayer AFM with $N_l=20$. The gapped surface state is labeled by orange lines. (h) The χ_{me} approaches $e^2/2h$ as the (even) number of layer goes up. Parameters: $A=1.4, B=1, M_0=1, m_z=0.3$. The temperature is set to be $k_BT=0.02$.

and $\delta_{\Delta}\Omega$ terms vanish because of they are full derivative of m and Ω .

Additionally, we can also get the electric Hall effect

$$\frac{d\sigma_H}{d\Delta} = \frac{e^2}{\hbar} \sum_n \int \frac{d^2 \mathbf{k}}{(2\pi)^2} (\mathcal{B}_{n\mathbf{k}} f'_{n\mathbf{k}} + \delta_\Delta \Omega_{n\mathbf{k}} f_{n\mathbf{k}})$$
 (6)

It describes how the Hall effect can be induced by the electric field Δ . The second term in Eq. (6) vanishes for the antiferromagnets with zero Berry curvature as discussed previously.

Example 1: monolayer $Ca(CoN)_2$.—To illustrate the ME effect induced by the SBCD and SOMD, we employ the low-energy effective model of monolayer Ca(CoN)2 [39]. As shown in Fig. 2(a), the electronic states in different valleys exhibit opposite layer polarization. The electronic states with opposite spin polarization (residing in different valleys) also possess opposite layer polarization, leading to a valley-mediated spin-layer locking. For monolayer Ca(CoN)2, the magnetic point group of the X and Y valleys is m'm'2. Within the basis (φ_t, φ_b) , the effective Hamiltonian at a given valley can be expressed as

$$H_X = \Delta \tau_z + v_1 k_x \tau_x + v_2 k_y \tau_y \tag{7}$$

$$H_Y = -\Delta \tau_z + v_1 k_y \tau_x - v_2 k_x \tau_y \tag{8}$$

Here the X and Y valleys are related by $C_{4z}\mathcal{PT}$ symmetry. We can analytically derive the SBCD as well

as SOMD for each valley separately. For X valley, the SBCD for the conduction/valence band is given by

$$\mathcal{B}_{c/v} = -\frac{v_1 v_2 \Delta^2}{2(\Delta^2 + v_1^2 k_x^2 + v_2^2 k_y^2)^2} \tag{9}$$

and the SOMD for the conduction/valence band is given by

$$\mathcal{M}_{c/v} = \mp \frac{e}{2\hbar} \frac{v_1 v_2 \Delta}{(\Delta^2 + v_1^2 k_x^2 + v_2^2 k_y^2)^{3/2}}$$
(10)

The quantities \mathcal{B} and \mathcal{M} have the same signs for the Y valley due to $C_{4z}\mathcal{PT}$ symmetry. In Fig. 2(b), we plot the momentum-space distribution of \mathcal{B}_{vk} for the X valley. The integral of \mathcal{B}_{vk} yields the ME coefficient $\chi_{\text{me}} = e^2/2h$. Note that this value is for a continuum model where the momentum integral extends to infinity; in a real tight-binding model with a periodic Brillouin zone, χ_{me} will be smaller.

As displayed in Fig. 2(c), we evaluate $\chi_{\rm me}$ as a function of Fermi energy μ . In the insulating regime, $\chi_{\rm me}$ is solely contributed by the Fermi-sea term \mathcal{B}_{k} , while in the metallic regime, the Fermi-surface term \mathcal{M}_{k} also arises. The sign of the Fermi-surface term is opposite for the conduction and valence bands because the orbital magnetic moment has the same sign in both, leading to $\mathcal{M}_{ck} = -\mathcal{M}_{vk}$. In contrast, the electric Hall effect is purely a Fermi-surface effect governed by the SBCD \mathcal{B}_{k} ,

as shown in Fig. 3(d). In this case, the sign of $d\sigma_H/d\Delta$ is the same for the conduction and valence bands, since $\mathcal{B}_{ck} = \mathcal{B}_{vk}$. It is worth noting that the spin magnetic moment can also give rise to the ME coupling as a Fermi-surface effect, while in this work we focus on the orbital origin.

Example 2: topological antiferromagnet multilayers.— To further explore the longitudinal ME effect and electric Hall effect, we take a second example by examining a bilayer magnetic insulator, as shown in Fig. 3(a). The corresponding tight-binding model Hamiltonian for 3D topological insulator can be expressed as [40, 41]

$$H_0 = \sum_{i=1,2,3,4,5} d_i(\mathbf{k}) \Gamma_i \tag{11}$$

where $d(\mathbf{k}) = (-A\sin k_x, -A\sin k_y, 0, M_0 - 6B + 2B(\cos k_x + \cos k_y + \cos k_z), -A\sin k_z)$ and $\Gamma = (\sigma_x s_x, \sigma_x s_y, \sigma_y s_0, \sigma_z s_0, \sigma_x s_z)$. Here σ and s denote the orbital and spin degree of freedom. The Hamiltonian for each layer is

$$h_0 = -A(\sin k_x \Gamma_1 + \sin k_y \Gamma_2) + [M_0 - 6B + 2B(\cos k_x + \cos k_y)]\Gamma_4$$
(12)

and the interlayer coupling term $T = -iA\Gamma_5/2 + B\Gamma_4$. Therefore, the model Hamiltonian for the antiferromagnet bilayer is given by

$$H_{tb} = \begin{pmatrix} h_0 + m_z \sigma_0 s_z & T \\ T^{\dagger} & h_0 - m_z \sigma_0 s_z \end{pmatrix}.$$
 (13)

where m_z denotes the layer-dependent exchange field characerizing the interlayer AFM order. This model can describe the essential physics of bilayer MnBi₂Te₄ [42]. Throughout this work we take the parameters $A = 1.4, B = 1, M_0 = 1, m_z = 0.3$ to illustrate the core physics.

We first study the bilayer case $(N_l = 2)$, as illustrated in Fig. 3(a). The band structure is shown in Fig. 3(b), with valence bands labeled 1 and 2. The momentumspace distribution of the SBCD for bands 1 and 2 is plotted in Fig. 3(c) and (d), respectively. This reveals that band 1 provides the dominant contribution to the orbital ME coupling, while the effect from band 2 is minor. This distinction can be understood from the significantly larger layer polarization of band 1. Using Eq. (5), we evaluate $\chi_{\rm me}$ as a function of the Fermi level μ in Fig. 3(e). The SBCD contributes to a Fermi-sea ME coupling with a non-quantized value of $\chi_{\rm me} \approx 0.72$. This deviation from quantization occurs because finite interlayer coupling results in a layer polarization $\langle p \rangle \neq 1/2$ for each layer. Notably, $\chi_{\rm me}$ has the same sign for the conduction and valence bands because $\mathcal{M}_{ck} = \mathcal{M}_{vk}$ in this system. We further calculate the electric Hall effect (or layer Hall effect) in Fig. 3(f). As expected for a Fermi-surface effect, $d\sigma_H/d\Delta$ stems from the SBCD and

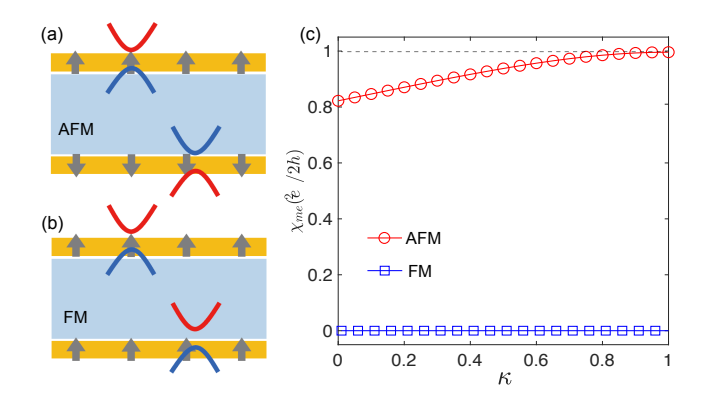


FIG. 4. (a) Schematic for an axion insulator with gapped surface state. The Dirac mass of top and bottom layers are opposite. (b) The FM bilayer with the quantum anomalous Hall state with the same Dirac mass for two layers. (c) χ_{me} as a function of κ . When $\kappa = 1$, the interlayer coupling vanishes.

vanishes in the insulating regime. Finally, we consider systems beyond the bilayer. Figure 3(g) shows the band structure for $N_l = 20$, where the low-energy gapped surface states induced by m_z are highlighted in orange. In Fig. 3(h), we plot the evolution of the ME coefficient $\chi_{\rm me}$ with increasing layer number N_l . We observe that $\chi_{\rm me}$ clearly approaches the quantized value of $e^2/2h$ in the large-thickness limit.

Multilayer magnetic totopogical insulators (MTI) have the gapped surface state localized on the top and bottom surfaces. Therefore, we can adopt an effective "bilayer" Hamiltonian, yielding

$$H_{eff} = \hbar v_0 (k_y s_x - k_x s_y) \tau_z + (1 - \kappa) m(\mathbf{k}) \tau_x + h_M$$
 (14)

Here we take $\hbar v_0 = 2eV \cdot \mathring{A}$. The interlayer coupling is given by $m(\mathbf{k}) = m_0 - m_1(k_x^2 + k_y^2)$ with parameters $m_0 = -10\,\mathrm{meV}$ and $m_1 = 20\,\mathrm{eV} \cdot \mathring{A}^2$. Here, s and τ are the Pauli matrices acting on the spin and layer subspaces, respectively. For the antiferromagnetic (AFM) bilayer, the magnetization term is $h_M = m_z s_z \tau_z$, while for the ferromagnetic (FM) bilayer it is $h_M = m_z s_z \tau_0$. This leads to opposite Dirac masses in the AFM case and identical Dirac masses in the FM case, as illustrated in Fig. 4(a) and (b). We note that the AFM bilayer models even-layer magnetic topological insulators (MTIs), whereas the FM bilayer models odd-layer MTIs [32]. The parameter κ controls the interlayer coupling strength, where $\kappa = 1$ corresponds to effectively decoupled layers.

Focusing on the Fermi-sea term from $\mathcal{B}_{n\mathbf{k}}$, we evaluate $\chi_{\rm me}$ for both AFM and FM cases. As shown in Fig. 4(c), $\chi_{\rm me}$ for the AFM bilayer saturates to the half-quantized value $e^2/2h$ as κ approaches 1, where the two layers are effectively decoupled. This quantization arises because the Berry curvature integral for a massive Dirac cone on the top/bottom layer is $\pm 1/2$, and the corresponding layer polarization is $\langle p \rangle = \pm 1/2$. Substituting these

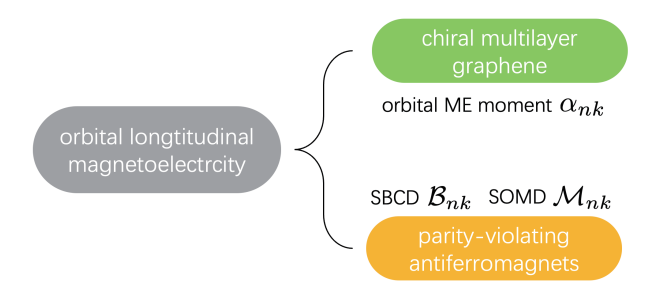


FIG. 5. summary of the origin of orbital magnetoelectricity in two representative systems: in chiral-stacked multilayer graphene, the effect is governed by the orbital ME moment α_{nk} , while in parity-violating antiferromagnets, it is dominated by the SBCD and SOMD, which is the primary focus of this work.

values into Eq. (5) directly yields $\chi_{\rm me} = e^2/2h$. In contrast, $\chi_{\rm me}$ vanishes for the FM bilayer for all values of κ , which occurs because the SBCD contributions from the top and bottom layers are equal in magnitude but opposite in sign, leading to perfect cancellation.

Finally, we would like to connect our theory to the topological ME effect within Chern-Simons theory. The topological ME response in an antiferromagnetic topological insulator is described by the topological θ -term

$$S_{\theta} = \frac{\theta}{2\pi} \frac{e^2}{h} \int d^3x \, dt \, \boldsymbol{E} \cdot \boldsymbol{B}, \tag{15}$$

where E and B are the conventional electromagnetic fields inside the insulator, and θ is a dimensionless pseudoscalar parameter defined modulo 2π . Physically, θ has an explicit microscopic expression as a momentum-space Chern-Simons form [15]. This parameter describes three fundamental physical phenomena: (i) The electric polarization induced by a small magnetic field. (ii) The orbital magnetization induced by a small electric field. (iii) A quantized, dissipationless surface Hall conductivity $\sigma_H = e^2/2h$.

In contrast, for quasi-2D layered systems, we find that an analogous θ_{2D} is determined by the integrated SBCD

$$\theta_{2D} = \sum_{n \in occ} \int d^2 \mathbf{k} \, \mathcal{B}_{n\mathbf{k}}, \tag{16}$$

a relation that holds generally for quasi-2D parity-violating antiferromagnetic insulators. While the surface Hall effect is not well-defined in atomically thin systems, we show that \mathcal{B}_{nk} nonetheless gives rise to a measurable electric Hall effect, as derived in Eq. (6).

Conclusion and discussion.—In summary, in this work we have studied that the interplay between Berry phase effects and stacking order in quasi-2D layered materials gives rise to a distinct orbital ME effect, differing fundamentally from known mechanisms in 3D systems. We

have identified the SBCD and SOMD as the key quantities governing this ME response in parity-violating antiferromagnets. This theoretical framework was demonstrated using two illustrative models.

As shown in Fig. 4 and derived from the general formula of Eq. (1), we have clarified the different microscopic origins of the orbital ME effect. In chiral multilayer graphene systems, the orbital ME moment α_{nk} determines the longitudinal ME coupling, as studied in Ref. [38] and supported by relevant experiments [43, 44]. In contrast, the SBCD and SOMD govern the longitudinal ME coupling in antiferromagnets such as $Ca(CoN)_2$ and $MnBi_2Te_4$. This work establishes a unified picture of the orbital ME effect in layered van der Waals materials. The general formalism developed here can be readily incorporated into first-principles calculations, providing a pathway for the quantitative prediction and design of ME phenomena in low-dimensional quantum materials.

Acknowledgement.—We are grateful to Justin C. W. Song, Yugui Yao, and X. C. Xie for fruitful discussion. J.X.H. was supported by the postdoctoral fellowship of Nanyang Technological University and Hong Kong University of Science and Technology.

- * jhuphy@ust.hk
- [1] G. Catalan, Applied Physics Letters 88 (2006).
- [2] R. Gupta and R. Kotnala, Journal of Materials Science 57, 12710 (2022).
- [3] K. Mori and M. Wuttig, Applied Physics Letters 81, 100 (2002).
- [4] H. Katsura, A. V. Balatsky, and N. Nagaosa, Physical review letters 98, 027203 (2007).
- [5] S. Fusil, V. Garcia, A. Barthélémy, and M. Bibes, Annual Review of Materials Research 44, 91 (2014).
- [6] H. Béa, M. Gajek, M. Bibes, and A. Barthélémy, Journal of Physics: Condensed Matter 20, 434221 (2008).
- [7] M. Trassin, Journal of Physics: Condensed Matter 28, 033001 (2015).
- [8] A. Iyama and T. Kimura, Physical Review B—Condensed Matter and Materials Physics 87, 180408 (2013).
- [9] J. Wang, J. Neaton, H. Zheng, V. Nagarajan, S. Ogale,
 B. Liu, D. Viehland, V. Vaithyanathan, D. Schlom,
 U. Waghmare, et al., science 299, 1719 (2003).
- [10] C.-Y. Kuo, Z. Hu, J. Yang, S.-C. Liao, Y. Huang, R. Vasudevan, M. Okatan, S. Jesse, S. V. Kalinin, L. Li, et al., Nature communications 7, 12712 (2016).
- [11] M. Zhu, Z. Zhou, B. Peng, S. Zhao, Y. Zhang, G. Niu, W. Ren, Z.-G. Ye, Y. Liu, and M. Liu, Advanced Functional Materials 27, 1605598 (2017).
- [12] J. H. Lee, L. Fang, E. Vlahos, X. Ke, Y. W. Jung, L. F. Kourkoutis, J.-W. Kim, P. J. Ryan, T. Heeg, M. Roeckerath, et al., Nature 466, 954 (2010).
- [13] S. Zhong, J. E. Moore, and I. Souza, Physical review letters 116, 077201 (2016).
- [14] W.-Y. He and K. Law, Physical Review Research 2, 012073 (2020).

- [15] A. M. Essin, J. E. Moore, and D. Vanderbilt, Physical review letters 102, 146805 (2009).
- [16] J. Wang, B. Lian, X.-L. Qi, and S.-C. Zhang, Physical Review B 92, 081107 (2015).
- [17] N. Sivadas, S. Okamoto, X. Xu, C. J. Fennie, and D. Xiao, Nano letters 18, 7658 (2018).
- [18] P. Jiang, C. Wang, D. Chen, Z. Zhong, Z. Yuan, Z.-Y. Lu, and W. Ji, Physical Review B 99, 144401 (2019).
- [19] Z. Sun, Y. Yi, T. Song, G. Clark, B. Huang, Y. Shan, S. Wu, D. Huang, C. Gao, Z. Chen, et al., Nature 572, 497 (2019).
- [20] C. Lei, B. L. Chittari, K. Nomura, N. Banerjee, J. Jung, and A. H. MacDonald, Nano Letters 21, 1948 (2021).
- [21] Y. Deng, Y. Yu, M. Z. Shi, Z. Guo, Z. Xu, J. Wang, X. H. Chen, and Y. Zhang, Science 367, 895 (2020).
- [22] J. Li, Y. Li, S. Du, Z. Wang, B.-L. Gu, S.-C. Zhang, K. He, W. Duan, and Y. Xu, Science advances 5, eaaw5685 (2019).
- [23] M. Otrokov, I. P. Rusinov, M. Blanco-Rey, M. Hoffmann, A. Y. Vyazovskaya, S. V. Eremeev, A. Ernst, P. M. Echenique, A. Arnau, and E. V. Chulkov, Physical review letters 122, 107202 (2019).
- [24] S. Li, M. Gong, S. Cheng, H. Jiang, and X. Xie, National Science Review 11, nwad262 (2024).
- [25] A. Gao, S.-W. Chen, B. Ghosh, J.-X. Qiu, Y.-F. Liu, Y. Onishi, C. Hu, T. Qian, D. Bérubé, T. Dinh, et al., Nature Electronics 7, 751 (2024).
- [26] A. Gao, Y.-F. Liu, C. Hu, J.-X. Qiu, C. Tzschaschel, B. Ghosh, S.-C. Ho, D. Bérubé, R. Chen, H. Sun, et al., Nature 595, 521 (2021).
- [27] A. Gao, Y.-F. Liu, J.-X. Qiu, B. Ghosh, T. V. Trevisan, Y. Onishi, C. Hu, T. Qian, H.-J. Tien, S.-W. Chen, et al., Science 381, 181 (2023).
- [28] N. Wang, D. Kaplan, Z. Zhang, T. Holder, N. Cao, A. Wang, X. Zhou, F. Zhou, Z. Jiang, C. Zhang, et al., Nature 621, 487 (2023).
- [29] X. Liu, A. P. Pyatakov, and W. Ren, Physical Review Letters 125, 247601 (2020).

- [30] J.-X. Qiu, B. Ghosh, J. Schütte-Engel, T. Qian, M. Smith, Y.-T. Yao, J. Ahn, Y.-F. Liu, A. Gao, C. Tzschaschel, et al., Nature, 1 (2025).
- [31] C. Lei, P. T. Mahon, C. M. Canali, and A. MacDonald, Physical Review Letters 133, 246607 (2024).
- [32] R. Mei, Y.-F. Zhao, C. Wang, Y. Ren, D. Xiao, C.-Z. Chang, and C.-X. Liu, Physical review letters 132, 066604 (2024).
- [33] N. Nagaosa, J. Sinova, S. Onoda, A. H. MacDonald, and N. P. Ong, Reviews of modern physics 82, 1539 (2010).
- [34] D. Xiao, M.-C. Chang, and Q. Niu, Reviews of modern physics 82, 1959 (2010).
- [35] I. Sodemann and L. Fu, Physical review letters 115, 216806 (2015).
- [36] J. Shi, G. Vignale, D. Xiao, and Q. Niu, Physical review letters 99, 197202 (2007).
- [37] D. Ceresoli, T. Thonhauser, D. Vanderbilt, and R. Resta, Physical Review B—Condensed Matter and Materials Physics 74, 024408 (2006).
- [38] J.-X. Hu and J. C. Song, arXiv preprint arXiv:2503.07822 (2025).
- [39] R.-W. Zhang, C. Cui, R. Li, J. Duan, L. Li, Z.-M. Yu, and Y. Yao, Physical Review Letters 133, 056401 (2024).
- [40] L. Fu, C. L. Kane, and E. J. Mele, Physical review letters 98, 106803 (2007).
- [41] H. Jiang, Z. Qiao, H. Liu, and Q. Niu, Physical Review B—Condensed Matter and Materials Physics 85, 045445 (2012).
- [42] D. Zhang, M. Shi, T. Zhu, D. Xing, H. Zhang, and J. Wang, Physical review letters 122, 206401 (2019).
- [43] T. Han, Z. Lu, G. Scuri, J. Sung, J. Wang, T. Han, K. Watanabe, T. Taniguchi, L. Fu, H. Park, et al., Nature 623, 41 (2023).
- [44] J. Deng, J. Xie, H. Li, T. Taniguchi, K. Watanabe, J. Shan, K. F. Mak, and X. Liu, arXiv preprint arXiv:2508.15909 (2025).